Research Article | Vol. 26, No. 21 | 15 Oct 2018 | OPTICS EXPRESS 26907
Optics EXPRESS

Highly stable, 15 W, few-cycle, 65 mrad CEP-noise mid-IR OPCPA for statistical physics

NICOLAS THIRÉ,[1,*] RAMAN MAKSIMENKA,[1] BÁLINT KISS,[2] CLÉMENT FERCHAUD,[1] GRÉGORY GITZINGER,[1] THOMAS PINOTEAU,[1] HERVÉ JOUSSELIN,[1] SEBASTIAN JAROSCH,[3] PIERRE BIZOUARD,[1] VITTORIO DI PIETRO,[1] ERIC CORMIER,[2] KÁROLY OSVAY,[2] AND NICOLAS FORGET[1]

[1]*Fastlite, 165 route des cistes 06600, Antibes, France*
[2]*ELI-HU Non-Profit Ltd, Dugonics tér 1 6720 Szeged, Hungary*
[3]*Imperial College London, South Kensington Campus, London SW7 2AZ, UK*
**nicolas.thire@fastlite.com*

Abstract: We demonstrate a 100 kHz optical parametric chirped-pulse amplifier delivering under 4-cycle (38 fs) pulses at ~3.2 µm with an average power of 15.2 W with a pulse-to-pulse energy stability <0.7% rms and a single-shot CEP noise of 65 mrad RMS over 8h. This source is continuously monitored, by using a fast 100 kHz data acquisition device, and presents an extreme stability, in the short and long terms.

1. Introduction

The advent of diode-pumped ytterbium-doped solid-state lasers has revolutionized femtosecond technologies [1] and strong-field physics not only because of their compactness and power scaling capabilities, but also because of versatile repetition rates and unmatched energy stability. The latter results from a combination of multiple favorable factors, either linked to the physical properties of ytterbium ions (long lifetime, simple electronic structure, relatively large gain bandwidth and small quantum defects) or to the technological aspects (compatibility with large set of host materials into fiber, bulk, slab, and thin-disk architectures and direct pumping by cost-effective laser diodes), allowing efficient and powerful laser amplification at multi-kHz to MHz repetition rates under steady-state pumping conditions. This technology, couple to the work on parametric amplification of ultrashort pulses [2], has set off the development of high-repetition rate optical parametric chirped-pulse amplifiers (OPCPA), especially in the mid-infrared range [3–11] where high repetition rate helps to counteract the rather low count rate of strong-field physics experiments such as COLTRIMS [12], reaction microscope [13], or conversion yield (X-UV generation [14]).

Energy stabilities well below the ~1% threshold, both shot-to-shot and long-term, unravel the potential of nonlinear optics to broaden bandwidths, shift wavelengths, generate or amplify light, without sacrificing the necessary prerequisites of deterministic experimental science: reproducibility and control of physical parameters. High-repetition rate sources also open the path to statistical analysis of large sets of data, an approach seldom used in strong-field physics so far because of the insufficient reproducibility of the intensity and/or electric field of short pulses.

In this paper, we exemplify such an approach by demonstrating an Ytterbium-pumped 100-kHz OPCPA generating few-cycle pulses at ~3.2 µm with a pulse energy of 152-µJ, a duration of 40-fs and a Strehl ratio >0.8. Compared to our previous publication [10], the output energy/power was increased by a factor >4 while maintaining or improving the other optical characteristics. Apart from this power upgrade, we present a complete long-term characterization of the output beam: a shot-to-shot energy stability of 0.7% RMS, a pointing stability of ~10 µrad RMS, and a carrier-envelope phase (CEP) noise of ~65 mrad over more than ~3 billion successive shots (>8h). To date, this is the best recorded non-averaged CEP

#341720 https://doi.org/10.1364/OE.26.026907
Journal © 2018 Received 7 Aug 2018; revised 6 Sep 2018; accepted 6 Sep 2018; published 1 Oct 2018

Optics EXPRESS

stability for an amplified system, independently of the wavelength, pulse duration or repetition rate. This OPCPA also delivers the highest reported peak power (152 µJ/38.2 fs with 92% in the main peak ~3.7 GW) at 100 kHz within the 2-4 µm wavelength range without post-compression.

2. Architecture

The OPCPA is pumped by an Yb^{3+}-YAG, thin-disk, regenerative amplifier (Dira-200, Trumpf Scientific Lasers) seeded by a 40 MHz oscillator (Amplitude Systèmes) and a fiber pre-amplifier (Fastlite). This regenerative amplifier delivers 2 mJ pulses at the repetition rate of 100 kHz (average power of 200 W). The pulse duration at 1030 nm is 1.1 ps full-width at half-maximum (FWHM). Beam profile is close to Gaussian (measured M^2<1.3) and the typical pulse-to-pulse energy stability is ~1% rms. The scheme of the optical setup is represented on Fig. 1.

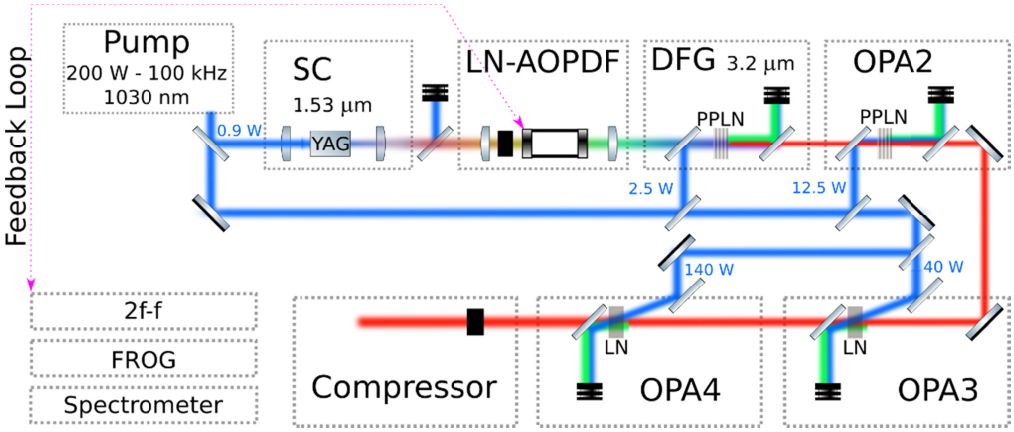

Fig. 1. Optical setup. SC: supercontinuum generation. LN-AOPDF: $LiNbO_3$ acousto-optic programmable dispersive filter. DFG: difference-frequency generation. OPA: optical parametric amplifier. 2f-f: collinear "2f-to-f" interferometer (CEP noise measurement). FROG: scanning second-harmonic frequency-resolved optical gating. PPLN: periodically poled MgO:$LiNbO_3$ crystal. LN: bulk $LiNbO_3$ crystal. Blue: 1.03 µm. Green: <2.06 µm. Red: >2.06 µm.

As already described with more details in [10], about 1 W is split from the main pump beam and spectrally-broadened up to ~2 µm in a 10 mm thick YAG crystal through filamentation. The 1.3-1.9 µm part of the supercontinuum is shaped by Lithium Niobate (LiNbO3) acousto-optic programmable dispersive filter (AOPDF, Dazzler, Fastlite) triggered at 100 kHz. The AOPDF is the heart of the dispersion scheme and cumulates five tasks: spectral selection, pulse-stretching to match the pump duration in the subsequent OPA stages, pre-compensation of the high-order spectral phase introduced along the entire system, CEP stabilization and control. In order to manage pulse duration at each stage, materials of different dispersion are used (Si with positive GDD, and CaF2 with negative GDD). This shaped seed is then amplified in a 1-mm MgO-doped Periodically Poled Lithium Niobate (PPLN) crystal (named DFG in Fig. 1). The generated idler pulse at ~3.2 µm, is selected and successively amplified in the subsequent OPA stages OPA2 (type-0, 0.7-mm MgO-PPLN crystal), OPA3 and OPA4 (both non-collinear, type-I, 1.5-mm, bulk LiNbO3 crystals). All the crystals are heat up to 120 °C. Doping level of MgO is 5% for the PPLNs. LNs are not doped. OPA3 and OPA4 are pumped by ~40 W (peak pump intensity of ~30 GW/cm2) and ~140 W (peak pump intensity of ~90 GW/cm2) respectively with an external angle of ~10°. The noncollinear geometry in the last two OPAs avoids the use of dichroic mirrors and helps to minimize nonlinear effects at these stages, sum frequency generations in particular. At the output of OPA4, the average power at ~3.2 µm is 16.5 W and the global quantum conversion

Optics EXPRESS

(including optical losses) of OPA4 is ~28%. In all OPA stages pump-seed synchronization is passive. The output beam is then expanded to ~10 mm FWHM and sent to a compressor made of 20 mm of bulk Silicon. The usable output power for experiments is 15.2W after the compressor. A 1-mm Sapphire plate serves as both output window and beam sampler (R = 7% from 2.5 to 4 µm on one side, R<1% on the other side. The reflected beam is divided and sent to embedded diagnostics for parallel monitoring of the shot-to-shot energy fluctuations (MCT photodiode), pulse duration (FROG, Frozzer, Fastlite), spectrum (1-5 µm scanning acousto-optic spectrometer, Mozza, Fastlite [15]) and CEP stability (2f-to-f interferometer equipped with a fast fringe detector, Fringeezz, Fastlite [16]). The output average power is measured behind the output window by a large-area water-cooled powermeter. To characterize the spatial beam profile, the output beam is attenuated by a set of reflections on AR-coated Silicon windows and sent to a thermal-infrared camera. Spatial phase is measured by a wavefront sensor (SWIR-SID4, Phasics) and the Strehl ratio is assessed by measuring the focal spot at the focus of a CaF2 lens (f = 500 mm at 3.2 µm). All measurements are done at full power and on the same day for the sake of completeness and comparison.

3. Spectrum

Figure 2(a) shows the output spectrum, acquired at the rate of one spectrum every minute over more than 8h. The spectrum extends from ~2.8 µm to 3.65 µm with a shape typical of saturated OPAs containing a dip at ~3.3 µm showing the onset of the back-conversion process. Spectral modulations in the 2.8-2.9 µm reveal absorption by water vapor and/or –OH contents in coatings and/or optics. Figure 2(a) is an overlay of 500 spectra. Given the very small fluctuations of the spectral intensity we compute and plot the probability density function of the spectral intensity rather than direct values. Note that the color scale is logarithmic and spans over several orders of magnitude. Figure 2(b) shows in a more conventional way the stability of the spectral shape over more than 8h.

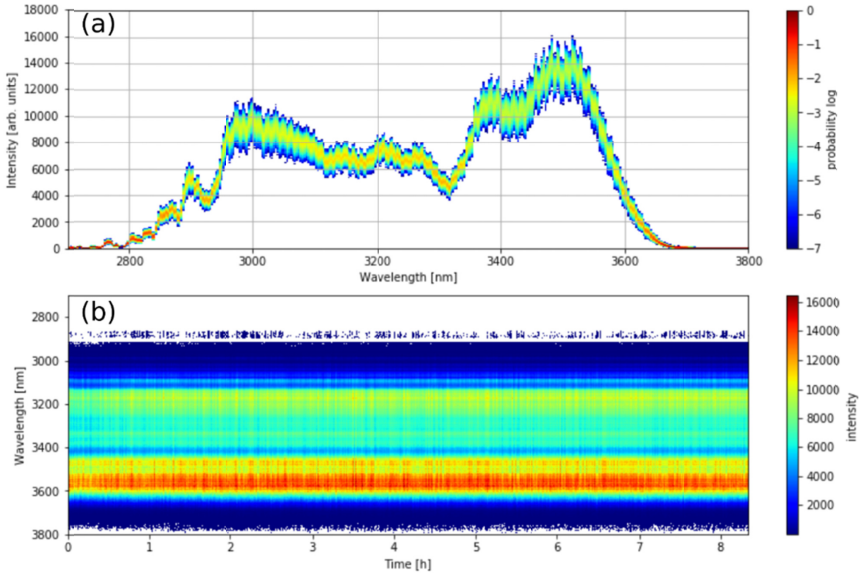

Fig. 2. (a): Overlay of 500 output spectra taken during 8 hours. Each column is a histogram of intensity computed for a particular wavelength. (b): Output spectrum as a function of time.

The system is optimized for 3.2 µm, but it is also important to notice its capability to be tuned from 2.5 µm (9.4 W – 85 fs FTL) to 3.8 µm (7.7 W – 140 fs FTL).

Optics EXPRESS

4. Pulse duration

Second-harmonic frequency-resolved optical gating (SH-FROG) is used to characterize the output pulses temporal profile [17]. A description of the optical setup can be found in [10]. A 1-mm Sapphire plate is inserted in the beam before the SH-FROG to take into account the dispersion of the output window. The retrieved pulse duration is 38.2 fs FWHM, for a Fourier-transform limit of 35.5 fs FWHM. The accuracy of the pulse reconstruction is assessed by computing the RMS reconstruction error (<1%, 160x160 calculation grid). Since the duration of an optical cycle at 3.2 µm is 10.7 fs, the pulses duration is less than four optical cycles.

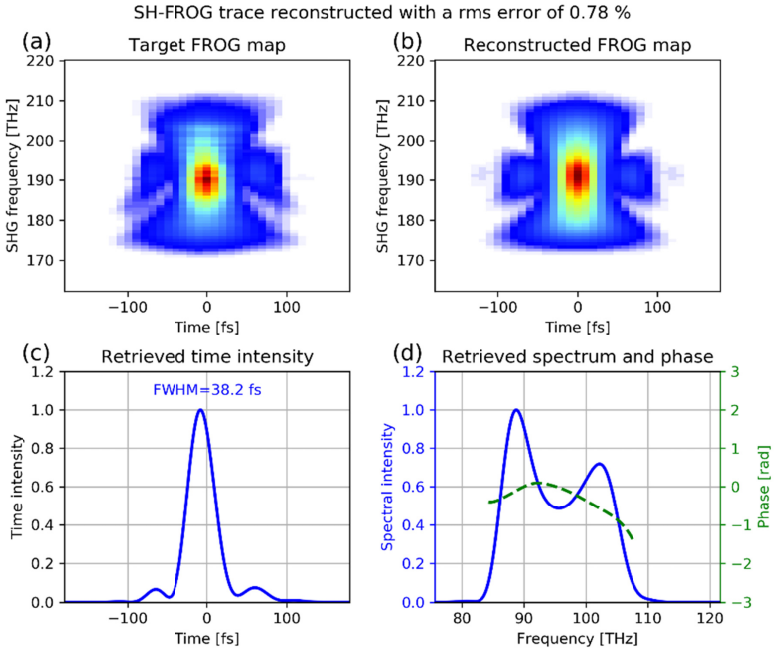

Fig. 3. (a) Experimental FROG trace. (b) Retrieved FROG trace. (c) Reconstructed time-dependent intensity. (d) Reconstructed spectrum and spectral phase.

5. Beam profile and Strehl ratio

The spatial beam profile at the output of the OPCPA is characterized by a customized uncooled micro-bolometer array (Pyroview, DIAS). The detector array is 640 x 480 pixels with a pixel pitch of 17 µm. The near-field beam profile (~1 m after the output window) is shown in Fig. 4. The beam is approximately Gaussian, with a diameter of ~14 mm at $1/e^2$. A fraction of the beam is sampled, attenuated and focused by a + 500 mm AR-coated plano-convex CaF_2 lens. The beam profile, at focus, is shown in Fig. 4, bottom left. To characterize the deviation from an ideal, diffraction limited beam, we compare the measured far field with the one computed from the near-field measurement assuming a perfectly flat spatial phase. Because of the unavoidable presence of a thermal background, a threshold at 5% (of peak counts) is applied to all measured beam profiles. Besides, a numerical filter equivalent to a physical round aperture of 29 mm is applied on the near-field profile to remove spurious contributions (halo from steering optics). Measured and computed widths at $1/e^2$ are 145 µm x 168 µm and 148 µm x 155 µm respectively, which indicate that the beam is actually close to its Fourier-transform limit. More quantitatively, the experimental peak fluence (far-field measurement) is 1.62 J/cm^2, whereas the theoretical peak fluence (deduced from the near-

Optics EXPRESS

field beam profile) is 1.97 J/cm^2. Defining the Strehl ratio as the relative loss of peak fluence at focus induced by spatial phase aberrations, provides a value of ~0.82. Another measurement of the Strehl ratio is performed with a wavefront sensor (SID4, Phasics) leading to a calculated value of 0.87, in good agreement with our experiment. The related M^2 value, also deduced from the wavefront measurements is ~1.40.

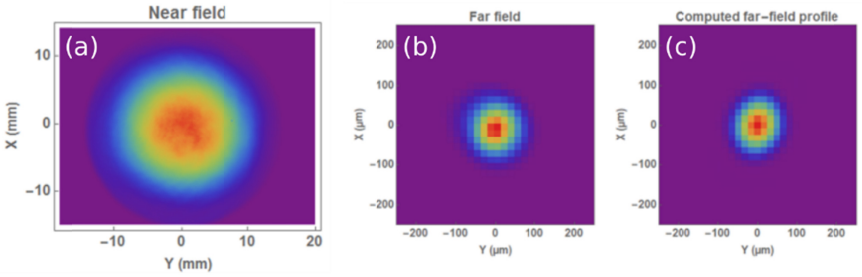

Fig. 4. Beam profile measured in near field (a) and far field (b). Computed far field (c).

Beam pointing fluctuation is defined as the RMS displacement of the beam barycenter in the far-field and was also measured over 8h. The RMS beam deviation is 3.1 µm along the X-direction and 4.8 µm along the Y-direction. The deduced beam pointing stability is ~0.02 times the beam divergence in the X- and ~0.03 in the Y-direction. Given the focal length of the focusing lens (500 mm), the beam pointing stability is <10 µrad RMS in both directions.

6. CEP fluctuations

Fluctuations of the carrier-envelope phase are characterized by "2f-to-f" interferometry [10,18]. Here, a collimated beam of 6 µJ first propagates through a thin type-I SHG crystal ($AgGaS_2$) and consequently generates a second harmonic beam that interferes with a stable continuum produced by focusing the beam in a YAG crystal. A 45° polarizer couples the polarizations of 2f and f. The spectral beating at ~1.55 µm between the continuum and the second harmonic is recorded by a fast fringe detector [16] during 8 hours at 10 kHz (integration time of 2 µs), meaning that an interferogram is acquired for one laser shot every ten pulses, for a total of 2.9 10^8 data points. A digital output (resolution of ~25 mrad: 8 bits digitalization over 2π) is used to feed back the CEP offset to the AOPDF at 10 kHz and correct for CEP fluctuations. The feedback loop is a simple proportional correction with a damping factor of 0.5. Figure 5 demonstrates the CEP stability measured for 8h. The CEP noise is 65 mrad RMS over the entire measurement. This extreme long-term stability and ultra-low noise of the CEP are result of the combination of the intrinsic passive stability of the "self-seeded DFG" process and the active feedback loop. As visible on Fig. 5, the discretization levels of the feedback (~25 mrad) starts to show up.

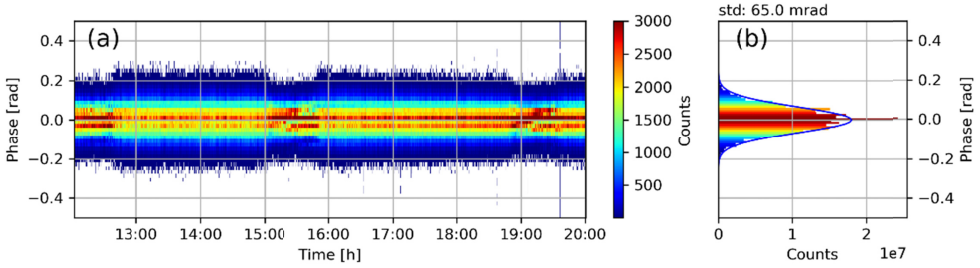

Fig. 5. Measured CEP noise over 8h (closed-loop). (a) Temporal evolution of CEP fluctuations: each column is a histogram of measured CEP offsets for 20000 shots (2 s at 10 kHz); (b) histogram of the total distribution of measured CEP offsets.

Optics EXPRESS

This excellent CEP stability and the capability to manipulate the electric field over a 25 mrad resolution is essential for controlling molecular systems with IR field [19] or, after a post compression stage, optoelectronics experiments [20].

7. Long-term power stability, shot-to-shot energy fluctuations

Average output power is measured every 10 s by a water-cooled, large area powermeter, with an integration time of 2 s. Figure 6 shows the output power after compression as a function of time, for a period of 12 hours. The time axis is local time in order to correlate these results with the CEP measurement (Figs. 5 and 8). The average power value is 15.2 W with a RMS stability of ± 0.7% over the full measurement. The break in the measurement at ~11:50 was caused by an external interlock event. After only a few minutes the full system was restarted and got back to the initial values within a few seconds.

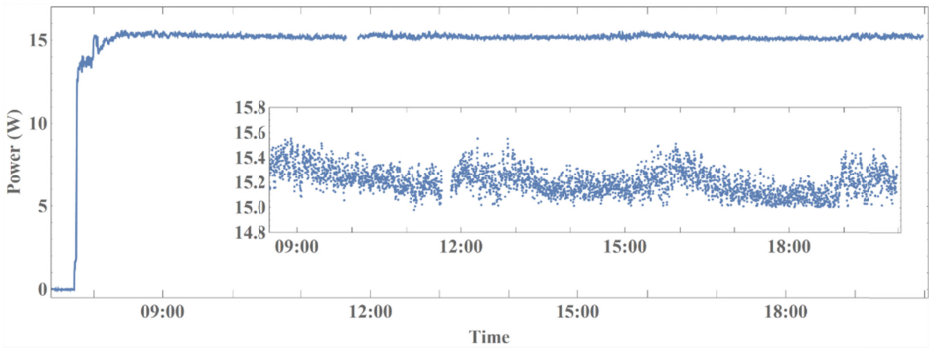

Fig. 6. Average power at the output of the OPCPA after the compression stage. Same data are shown with two scales: [7:20-20:00, 0-17 W] and inset: [8:30-20:00, 14.8-15.8 W].

In parallel, a large-area, TE-cooled, HgCdTe photodiode is used to monitor the output pulse-to-pulse energy. Given the high repetition rate and the high vertical resolution required to resolve low level of the energy fluctuations, an acquisition system has been specifically developed to acquire and log data values at 100 kHz with a dynamic range >40 dB. The combination of these two features allows the computation of statistical figures, and in particular energy fluctuations, with a precision well below 0.1%. This acquisition system (BigBrozzer, Fastlite) is designed to record the data from sixteen input channels simultaneously. Embedded in the OPCPA, it monitors continuously the pump beam position (4-quadrant detector) as well as the energies of pump, continuum, DFG and output beams.

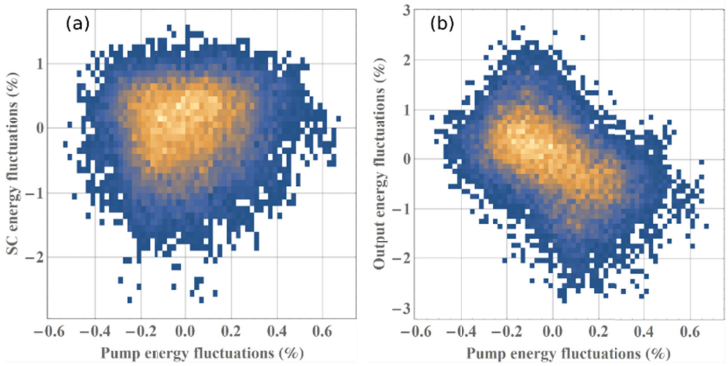

Fig. 7. (a) Supercontinuum (SC) energy fluctuations as a function of pump energy fluctuation (fluctuations relative to the average pulse energies). (b) Output energy fluctuations in function of pump energy fluctuations. Both plots are density functions corresponding to 20 000 successive pulses.

Optics EXPRESS

Figure 7 shows an example of the statistical approach. On Fig. 7(a) the relative fluctuations of the SC energy are plotted against the relative fluctuations of the pump energy. There is no clear correlation between these two data sets. One can still note that the SC energy looks clamped toward the highest energy values. This feature can probably be related to the self-stabilization regime reported in [21]. Figure 7(b) correlates similarly the fluctuations of the output energy versus the pump energy. There is a clear anti-correlation with a slope of approximately −4 showing that OPA4 operates in the saturation regime. In order to be able to save data for a long-period (around a month on a 32 Gb memory card), four parameters are computed and saved every second (i.e. calculated over 100 000 consecutive shots) for all input channels: the average value, the RMS value, the minimum value and the maximum value. Figure 8 compares over 8h the RMS CEP noise (closed-loop) with the following data: relative output pulse energy, relative pump energy, OPCPA RMS energy noise and pump RMS energy noise. The Spearman's rank correlation (or Spearman's rho) coefficients between the RMS CEP and the latter data are, respectively: + 0.48, −0.32, + 0.46 and −0.33. CEP appears to be mostly correlated to the output pulse energy rather than to the pump energy. Interestingly, the CEP noise is not only related to the RMS fluctuations (i.e. the best CEP stability is achieved when the system is the most stable) but also to the average pulse energy. This phenomenon may be explained by an intensity-phase coupling induced by the white-light generation stage of the 2f-to-f interferometer: as described in the section IV of [22], the strength of this intensity-phase coupling actually depends on the input energy level. This measurement also shows a weaker correlation between the pump energy and CEP noise. Beyond the correlation coefficient, a common periodic variation (cycle of 10-15 mn) is clearly visible. For the sake of completeness, it has to be mentioned than the abrupt drops of the output energy are linked to the start/stop of the cooling unit of the system.

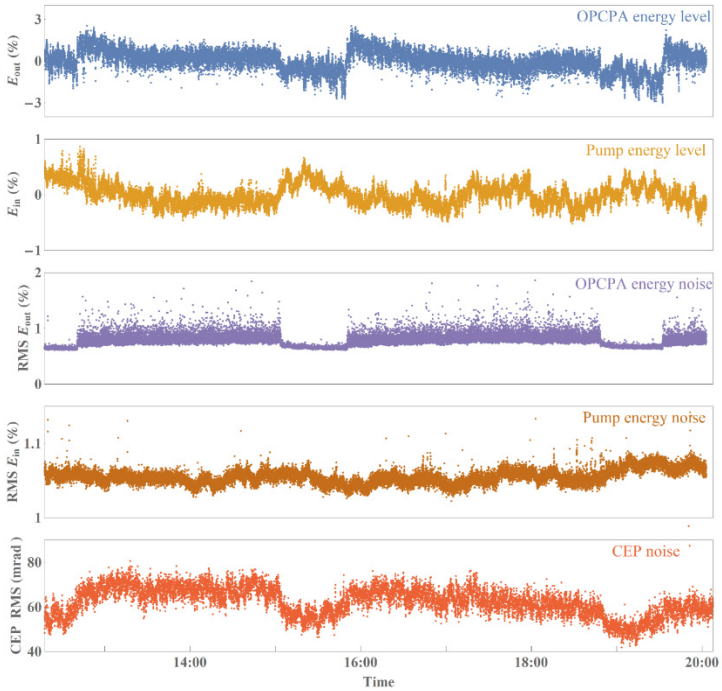

Fig. 8. From top to bottom, long term measurements of: relative OPCPA output energy, relative pump energy, RMS OPCPA energy fluctuations, RMS pump energy fluctuations, CEP noise (RMS). All data were acquired single-shot at 100 kHz (pump energy, OPCPA energy) or 10 kHz (CEP). The OPCPA and pump variations are relative to the average value computed over 8h.

Optics EXPRESS

Although the information deduced from Figs. 7 and 8 was predictable, the interest of the fast data acquisition device lies in the fact that for each shot, several experimental values can be correlated, both shot-to-shot and on the long-term. This is not only useful for understanding the physics of this OPCPA system, but also for analyzing the effect of laser parameters on scientific results. In the present case, this study tends to show that the stability of the CEP is ultimately limited by the stability of white-light generation stage of the 2f-to-f device through intensity-phase coupling. To a lesser extent, another contribution, linked to the pump energy, can be detected. This feature could also be a signature of an intensity-phase coupling but at the SC or DFG level.

8. Conclusion and prospects

We have characterized a 100-kHz, 3.2-µm, 15.2-W, 4-cycle OPCPA with an RMS energy/power stability < 0.7% and an RMS carrier-envelope phase noise of 65 mrad with no drift over eight consecutive hours, which corresponds to almost three billion pulses. We demonstrated that a peak intensity of 10^{15} W/cm^2 with a focal spot of 20 µm FWHM is reachable, making this source suitable to drive nonlinear strong-field processes like HHG up to keV energy level [23]. Coupled to the embedded multi-channel data acquisition device, this system is suitable for performing ultra-stable shot-to-shot measurements over a long-term, promising data accumulation difficult to reach with other sources demonstrated so far.

Funding

European Regional Development Fund (2.3.6-15-2015-00001); H2020 Marie Skłodowska-Curie Actions (641272).

References

1. H. Fattahi, H. G. Barros, M. Gorjan, T. Nubbemeyer, B. Alsaif, C. Y. Teisset, M. Schultze, S. Prinz, M. Haefner, M. Ueffing, A. Alismail, L. Vámos, A. Schwarz, O. Pronin, J. Brons, X. T. Geng, G. Arisholm, M. Ciappina, V. S. Yakovlev, D.-E. Kim, A. M. Azzeer, N. Karpowicz, D. Sutter, Z. Major, T. Metzger, and F. Krausz, "Third-generation femtosecond technology," Optica **1**(1), 45–63 (2014).
2. A. Dubietis, G. Jonušauskas, and A. Piskarskas, "Powerful femtosecond pulse generation by chirped and stretched pulse parametric amplification in BBO crystal," Opt. Commun. **88**(4–6), 437–440 (1992).
3. B. M. Luther, K. M. Tracy, M. Gerrity, S. Brown, and A. T. Krummel, "2D IR spectroscopy at 100 kHz utilizing a Mid-IR OPCPA laser source," Opt. Express **24**(4), 4117–4127 (2016).
4. A. Thai, M. Hemmer, P. K. Bates, O. Chalus, and J. Biegert, "Sub-250-mrad, passively carrier-envelope-phase-stable mid-infrared OPCPA source at high repetition rate," Opt. Lett. **36**(19), 3918–3920 (2011).
5. B. W. Mayer, C. R. Phillips, L. Gallmann, and U. Keller, "Mid-infrared pulse generation via achromatic quasi-phase-matched OPCPA," Opt. Express **22**(17), 20798–20808 (2014).
6. U. Elu, M. Baudisch, H. Pires, F. Tani, M. H. Frosz, F. Köttig, A. Ermolov, P. St.J. Russell, and J. Biegert, "High average power and single-cycle pulses from a mid-IR optical parametric chirped pulse amplifier," Optica **4**(9), 1024 (2017).
7. B. W. Mayer, C. R. Phillips, L. Gallmann, M. M. Fejer, and U. Keller, "Sub-four-cycle laser pulses directly from a high-repetition-rate optical parametric chirped-pulse amplifier at 3.4 µm," Opt. Lett. **38**(21), 4265–4268 (2013).
8. M. Mero, F. Noack, F. Bach, V. Petrov, and M. J. J. Vrakking, "High-average-power, 50-fs parametric amplifier front-end at 1.55 µm," Opt. Express **23**(26), 33157–33163 (2015).
9. P. Rigaud, A. Van de Walle, M. Hanna, N. Forget, F. Guichard, Y. Zaouter, K. Guesmi, F. Druon, and P. Georges, "Supercontinuum-seeded few-cycle mid-infrared OPCPA system," Opt. Express **24**(23), 26494–26502 (2016).
10. N. Thiré, R. Maksimenka, B. Kiss, C. Ferchaud, P. Bizouard, E. Cormier, K. Osvay, and N. Forget, "4-W, 100-kHz, few-cycle mid-infrared source with sub-100-mrad carrier-envelope phase noise," Opt. Express **25**(2), 1505–1514 (2017).
11. M. Neuhaus, H. Fuest, M. Seeger, J. Schötz, M. Trubetskov, P. Russbueldt, H. D. Hoffmann, E. Riedle, Z. Major, V. Pervak, M. F. Kling, and P. Wnuk, "10 W CEP-stable few-cycle source at 2 µm with 100 kHz repetition rate," Opt. Express **26**(13), 16074–16085 (2018).
12. R. Dörner, V. Mergel, O. Jagutzki, L. Spielberger, J. Ullrich, R. Moshammer, and H. Schmidt-Böcking, "Cold Target Recoil Ion Momentum Spectroscopy: a 'momentum microscope' to view atomic collision dynamics," Phys. Rep. **330**(2-3), 95–192 (2000).
13. J. Ullrich, R. Moshammer, A. Dorn, R. Dörner, L. Ph. H. Schmidt, and H. Schmidt-Böcking, "Recoil-ion and electron momentum spectroscopy: reaction-microscopes," Rep. Prog. Phys. **66**(9), 1463–1545 (2003).

Optics EXPRESS

14. A. D. Shiner, C. Trallero-Herrero, N. Kajumba, H.-C. Bandulet, D. Comtois, F. Légaré, M. Giguère, J.-C. Kieffer, P. B. Corkum, and D. M. Villeneuve, "Wavelength Scaling of High Harmonic Generation Efficiency," Phys. Rev. Lett. **103**(7), 073902 (2009).
15. G. Gitzinger, V. Crozatier, R. Maksimenka, S. Grabielle, N. Forget, S. Alisauskas, A. Pugzlys, A. Baltuska, B. Monoszlai, C. Vicario, and C. P. Hauri, "Multi-octave acousto-optic spectrum analyzer for mid-infrared pulsed sources," in CLEO: 2014, paper STh1N.5, OSA Technical Digest (2014).
16. F. Lücking, V. Crozatier, N. Forget, A. Assion, and F. Krausz, "Approaching the limits of carrier-envelope phase stability in a millijoule-class amplifier," Opt. Lett. **39**(13), 3884–3887 (2014).
17. D. J. Kane and R. Trebino, "Characterization of Arbitrary Femtosecond Pulses Using Frequency-Resolved Optical Gating," IEEE J. Quantum Electron. **29**(2), 571–579 (1993).
18. M. Kakehata, H. Takada, Y. Kobayashi, K. Torizuka, Y. Fujihira, T. Homma, and H. Takahashi, "Single-shot measurement of carrier-envelope phase changes by spectral interferometry," Opt. Lett. **26**(18), 1436–1438 (2001).
19. V. Wanie, H. Ibrahim, S. Beaulieu, N. Thiré, B. E. Schmidt, Y. Deng, A. S. Alnaser, I. V. Litvinyuk, X. M. Tong, and F. Légaré, "Coherent control of D 2 /H 2 dissociative ionization by a mid-infrared two-color laser field," J. Phys. B **49**(2), 025601 (2016).
20. M. Schultze, E. M. Bothschafter, A. Sommer, S. Holzner, W. Schweinberger, M. Fiess, M. Hofstetter, R. Kienberger, V. Apalkov, V. S. Yakovlev, M. I. Stockman, and F. Krausz, "Controlling dielectrics with the electric field of light," Nature **493**(7430), 75–78 (2012).
21. L. Indra, F. Batysta, P. Hříbek, J. Novák, Z. Hubka, J. T. Green, R. Antipenkov, R. Boge, J. A. Naylon, P. Bakule, and B. Rus, "Picosecond pulse generated supercontinuum as a stable seed for OPCPA," Opt. Lett. **42**(4), 843–846 (2017).
22. A. Baltuska, M. Uiberacker, E. Goulielmakis, R. Kienberger, V. S. Yakovlev, T. Udem, T. W. Hänsch, and F. Krausz, "Phase-controlled amplification of few-cycle laser pulses," IEEE J. Sel. Top. Quantum Electron. **9**(4), 972–989 (2003).
23. T. Popmintchev, M.-C. Chen, D. Popmintchev, P. Arpin, S. Brown, S. Ališauskas, G. Andriukaitis, T. Balčiunas, O. D. Mücke, A. Pugzlys, A. Baltuška, B. Shim, S. E. Schrauth, A. Gaeta, C. Hernández-García, L. Plaja, A. Becker, A. Jaron-Becker, M. M. Murnane, and H. C. Kapteyn, "Bright coherent ultrahigh harmonics in the keV x-ray regime from mid-infrared femtosecond lasers," Science **336**(6086), 1287–1291 (2012).